SCIENTIFIC REPORTS

OPEN

SUBJECT AREAS:
MOLECULAR SELF-ASSEMBLY
NANOPARTICLES
SURFACES, INTERFACES AND THIN FILMS
STRUCTURAL PROPERTIES

Received
22 May 2013

Accepted
22 August 2013

Published
10 September 2013

Correspondence and requests for materials should be addressed to J.J.L. (jianglin@ntu.edu.tw)

Self-assembled clay films with a platelet–void multilayered nanostructure and flame-blocking properties

Ya-Chi Wang[1], Ting-Kai Huang[1], Shih-Huang Tung[1], Tzong-Ming Wu[2] & Jiang-Jen Lin[1]

[1]Institute of Polymer Science and Engineering, National Taiwan University, Taipei 10617, Taiwan, [2]Department of Materials Science and Engineering, National Chung Hsing University, Taichung 40227, Taiwan.

Polymeric composite films with a high loading of nano-size silicates can hardly meet the increasingly stringent fireproof and smoke-free requirements during burning. Thus, it is desirable to prepare pure clay films that can block air, heat, and flame. Here we report an organic-free clay film capable of both flame- and heat-shielding. The film was prepared from the self-assembly of nanometer-thick silicate platelets derived from the exfoliation of natural clays. The self-assembled film has a highly regular multilayered nanostructure over a large area and an appreciable volume of air entrapped in between. The combination of regular structure and substantial air volume contributes to the low thermal conductivity and flame blocking property of the film. It was demonstrated that the film can shield flame over hour duration and prevent temperature rising on the backside of film. This remarkable clay film has a myriad of uses including gas barrier, heat insulator, and fireproof devices.

Bottom-up self-assembly on a nanometer scale is an emerging process that often uses surfactants or block copolymers as soft templates for shaping ordered structures and generally involves weak forces from non-covalent bonds[1–4]. As an alternative example, ionic plate-like silicate clays interact with hydrophilic polymers to produce hydrogels and nanostructure films with enhanced properties like mechanical strength, gas barrier property, and flame retardancy[5–8]. In hydrophobic polymers based nanocomposites, inorganic silicates are inherently incompatible with the organics; thus effective blends are largely limited by a small fraction of inorganic. Only a few reports describe polymeric composite films that contain a large fraction of silicate clays (over 30%) since dispersion becomes inhomogeneous and hinders the formation, scaling-up, and flexibility of films[9–16].

Recently, the demand for new fireproof materials is growing due to stringent fire regulations. Conventional polymeric materials that contain organic phosphorus additives as flame retardants can delay flame propagation only to some extent[17]. Although new developments in nanotechnology allow inorganics to be blended on a nanometer scale with organic polymers, these polymer composites with organic additives are less fireproof and are often impractical because of the smoke produced by burning organics[18–22]. Thus, it is highly desirable to prepare self-assembled films that contain a high proportion of silicates.

In recent work, we developed a method to exfoliate the pristine multilayered sodium montmorillonite (Na^+-MMT) into individual platelets, by overcoming the strong stacking forces between the platelets. In other words, the inherent structural units of platelet-to-platelet multilayers were completely delaminated into miniature nanoplatelets that can serve as the fundamental units for bottom-up assembly. In this process, nanoscale silicate platelets (NSPs) were extracted by a two-phase solvent system to a purity of nearly 100% inorganics[23]. The thin NSPs at nanometer thickness are highly dispersible in water, gel into fibril shapes over only 8 wt% concentration, and self-assemble into lengthy ordered structure after water evaporation[24]. We have also reported that both organically intercalated and exfoliated clays can self-assemble into various morphologies[25].

The isolation of randomized single platelets led us to the preparation of pure clay films and the study on their self-assembled nanostructures. By judiciously selecting the rate at which water evaporates and the surface of the substrate, we have successfully fabricated thin films with nearly 100% inorganic silicates. Formed from nanometer-thick platelets, the flexible NSP films remain dimensionally stable even when exposed to a flame. The unexpected ability of hundreds of layered NSP units to self-assemble allows us to prepare large-scale films by a water-drying process.

Results

Self-assembled NSP clay films. The miniaturization of natural clays was achieved by a previously developed process (Fig. 1a)[23]. Because of the large number of ions (18,000 sodium counter-ions per platelet) and the extreme aspect ratio (lateral dimensions of 100 × 100 nm^2 and a thickness of 1 nm), we could easily cast NSP suspensions into free-standing thin films by selecting the surface of the casting substrate and by controlling the rate of water evaporation. The NSP films were contaminated with less than 1 wt% of organic moieties, as measured by thermal gravimetric analysis (TGA) (see Supplementary Fig. S1 online). With such a high inorganic purity, the NSP films with a thickness of 5 μm had a flexibility of 2 mm in the minimum bend diameter of a cylindrical bend test and a transparency of 30–40% of visible light transmitted (Fig. 1b and see Supplementary Movie 1 online). It is noteworthy that the films could be scaled up to a large area such as 50 cm × 65 cm × 50 μm (Fig. 1c).

An important parameter for self-assembly is the geometric shape of the 1 nm platelets. The high aspect ratio made film forming easy and self-assembling regular, compared to MMT films prepared from pristine MMT clay units (which average 8–10 platelets per stack). SEM micrographs showed that a cross section of an MMT film has a wavy texture, while that of an NSP film has a flatter texture (Fig. 1d and 1e, respectively). The self-assembly and alignment of NSP films are conceptually illustrated in Supplementary Fig. S2 online. If the stacking direction of the platelets were affected by sedimentation under gravity, the texture of the NSP films would have been parallel to the surface of the earth rather than aligned with the surface of the substrate. However, all produced films have the same texture aligning parallel to the substrates which are placed at three different angles of 0°, 60°, and 90° with respect to the earth's surface. This result implies that the self-stacking of NSPs does not depend on the angle of the substrate with respect to gravity, but that it is predominantly determined by, initially, the forces between the substrate and the silicate platelets and, subsequently, the forces between platelets as they stack.

Characterization of nanostructures in the films by WAXRD. The NSP and the MMT films consist of the same kind of silicate platelets but different fundamental units of clay stacks and, in the case of NSP films, exfoliated nanoplatelets. Their differences in XRD diffraction peaks arise from the self-assembling of two distinctly different clay units. Using Scherrer's equation: $L = \lambda/(\beta\cos\theta)$, we calculated the thickness (L) of the fundamental units of the self-assembled films, where λ and β represent the X-ray wavelength and the integral half-width of reflection, respectively. The results in Table 1 show that the MMT films possess fundamental units that are 93–108 Å thick, which corresponds to the original clay stack of 8 silicate platelets for each unit, regardless of the film thickness (20 to 100 μm) and the temperature during self-assembling. In the NSP films, the stack units may be manipulated. For example, it was observed to be approximately 4 and 10 silicate platelets in unit stacks for the different 20 and 100 μm thicknesses, respectively.

The orientation at which the platelets stacked was determined from measurements of X-ray diffraction in two different planes, one along the z-axis, i.e., perpendicular to the film's surface; and the other along the x-y plane, i.e., parallel to the film's surface (Fig. 2a–2e and respective converted 1D profiles shown in Fig. 2f). The arrangement of the experiment is illustrated in Figure 2a. The ring-like diffraction patterns measured along the z-axis in the 2D images suggest no preferred orientation in the x-y plane for both the MMT and the NSP films (Fig. 2b and 2c, respectively). When measured along the x-y plane, the 2D images of the MMT and the NSP films (Fig. 2d and 2e, respectively) showed arc patterns instead of rings of (001) basal planes and thus confirmed the preferential

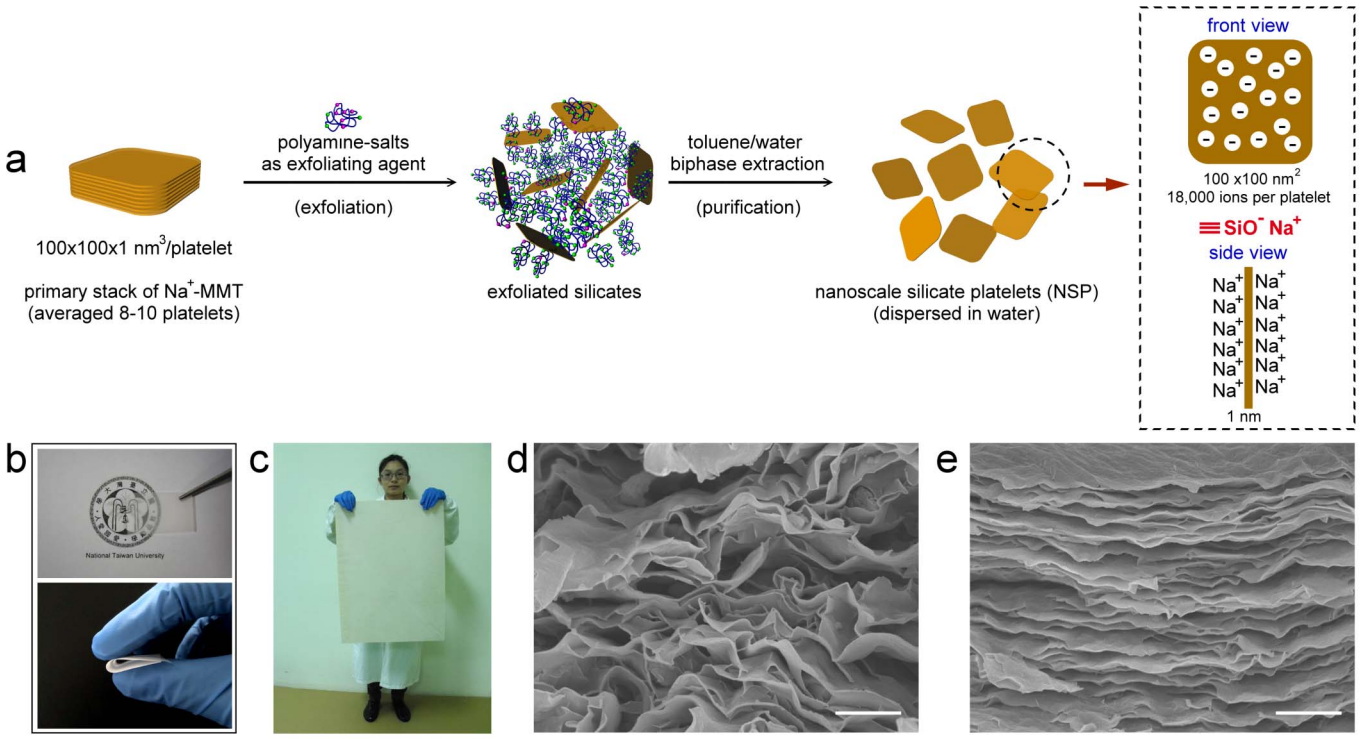

Figure 1 | Exfoliation of MMT clay stacks into random silicate platelets, images of clay films, and magnified views on their microstructures. (a) MMT clay stacks were exfoliated by using polyamine salts and were subsequently extracted and separated to produce NSPs in water. (b) An NSP film (5 μm thickness) showing a transparency of 30–40% of light. (c) Demonstration of a large-scale NSP film (50 cm × 65 cm and 50 μm thick), which is freely standing and uniform. (d) SEM image of a cross section of an MMT film (scale bar: 2 μm). (e) SEM image of a cross section of an NSP film (scale bar: 2 μm). Note: The author Ya-Chi Wang, whose image appears in Figure 1c, gives full permission for her image to be published online by the publisher of *Nature*.

Table 1 | Number of platelets constituting the fundamental stack in the clay films at different thicknesses (calculated from Scherrer's Equation)

Clay film	Temperature (°C)	Thickness (μm)	*d*-spacing (Å)	Correlation length (Å)	Platelets per stack
NSP	60	100	13.4	66.1	4–5
	60	20	13.4	59.4	4–5
	25	100	15.0	150	10–11
	25	20	14.9	63.8	4–5
MMT	60	100	12.6	94.9	7–8
	60	20	12.6	100	7–8
	25	100	12.7	108	8–9
	25	20	12.7	92.4	7–8

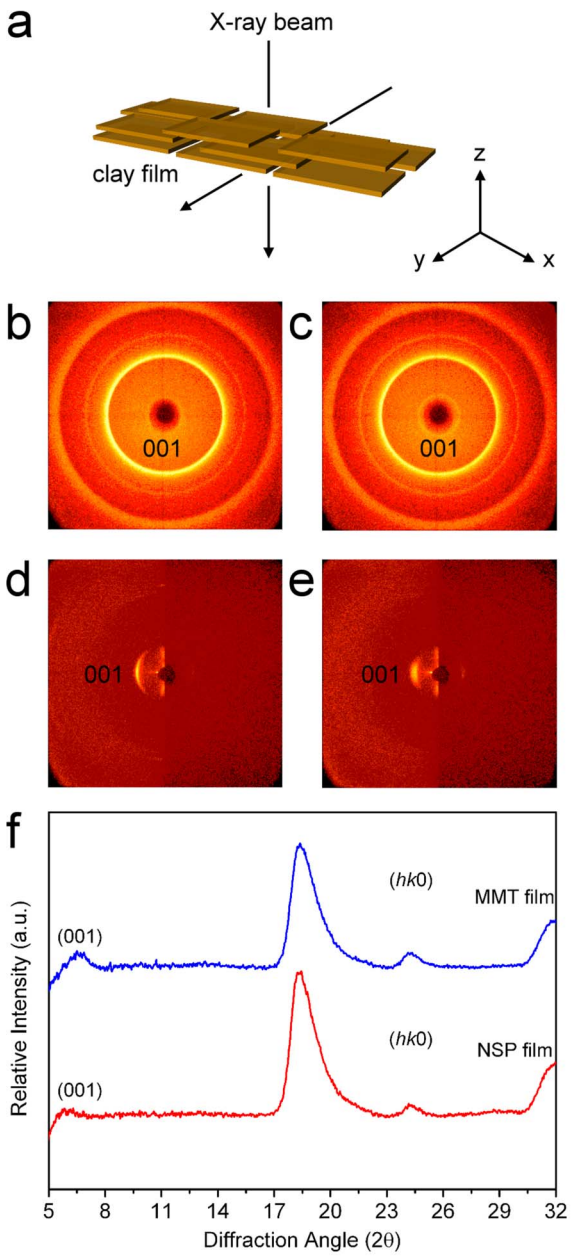

Figure 2 | Determination by 2D-XRD of the regularity of aligned units in the clay films. (a) Scheme of 2D-XRD. (b) and (c) 2D diffraction patterns along the *z*-axis for an MMT and NSP film, respectively. (d) and (e) 2D diffraction patterns along the *x*-*y* plane, respectively, for an MMT and NSP film, respectively. (f) 1D diffraction profiles for an MMT and an NSP film, showing 12.6 Å vs. 14.6 Å, respectively.

stacking of platelets along the *z*-axis. It is unusual that the diffraction intensities of the (001) basal planes are weaker than those of other planes at a higher 2θ, especially for the NSP films (Fig. 2f). All the peaks other than (001) planes are at identical positions for the MMT and NSP films, supposedly caused by (*hk*0) planes since the spacing of such planes would not be affected by the exfoliation treatments. The weak diffraction of (001) plane measured along *z*-axis implies that the majority of the platelets lie parallel to the surface. Furthermore, the barely visible (001) peak in the NSP films suggests that the stacking of platelets in the films is highly oriented, and this idea was further strengthened by the arc of the NSP films with a narrower azimuth angle.

The angle of diffraction provided additional information on the self-assembling of the silicate platelets. The 2θ of 7.0° and 6.0° for the MMT and the NSP films corresponds to a *d*-spacing of 12.6 and 14.6 Å, respectively (Fig. 2f). The increase of 2.0 Å in the *d*-spacing reflects the importance of exfoliating MMT stacks into NSPs, which have a less strained alignment of units over a large area of a film.

Multilayered nanostructure of alternating layers of platelets and voids. While water evaporates and the films self-assemble, pockets of air are trapped between neighboring platelets of the multilayered structures. The self-assembly into layered arrangement and ordered nanostructure will largely decide the formation of voids and density in the films[26,27]. We were able to estimate the volume percentage of voids by measuring the bulk density (in air) and the apparent density (in solvent after penetration). Two types of air voids could be identified and correlated to the nanostructures of stacked NSPs. The void that allows the solvent toluene to permeate is defined as a macro void, while a micro void is the volume impenetrable to solvent (Fig. 3). The total volumes of macro and micro voids were determined from the bulk density according to the procedure described in Methods, and the results were listed in Table 2. The bulk densities (in air) of the NSP and the MMT films are in the range of 1.5 and 2.1 g cm^{-3}, which are generally smaller than the reported 2.6 g cm^{-3} for bulk MMT[28]. The relatively low density of the NSP films implies the presence of entrapped air voids. It is noteworthy that, as the thickness of the NSP films increases, the apparent density slightly decreases, and the relative percentage of the macro voids to the total voids significantly decreases. These trends are attributed to the increased regularity of self-alignment. The observation is also consistent with the XRD measurements that the MMT films have the same apparent density regardless of thickness. The increasing regularity of self-assembling occurred only in the NSP films. Hence, the volume ratio of micro to macro voids could serve as an index for estimating the degree of orderly nanostructure. A greater index represents more regularity of the self-assembling structure. Overall, the wavy layers in the cross section and the ratio of micro to macro voids indicate a high degree of regularity in the nanostructure of NSP films.

The ability of the films to block a flame and heat. We examined clay films that were 20 μm thick for their ability to block a flame. A

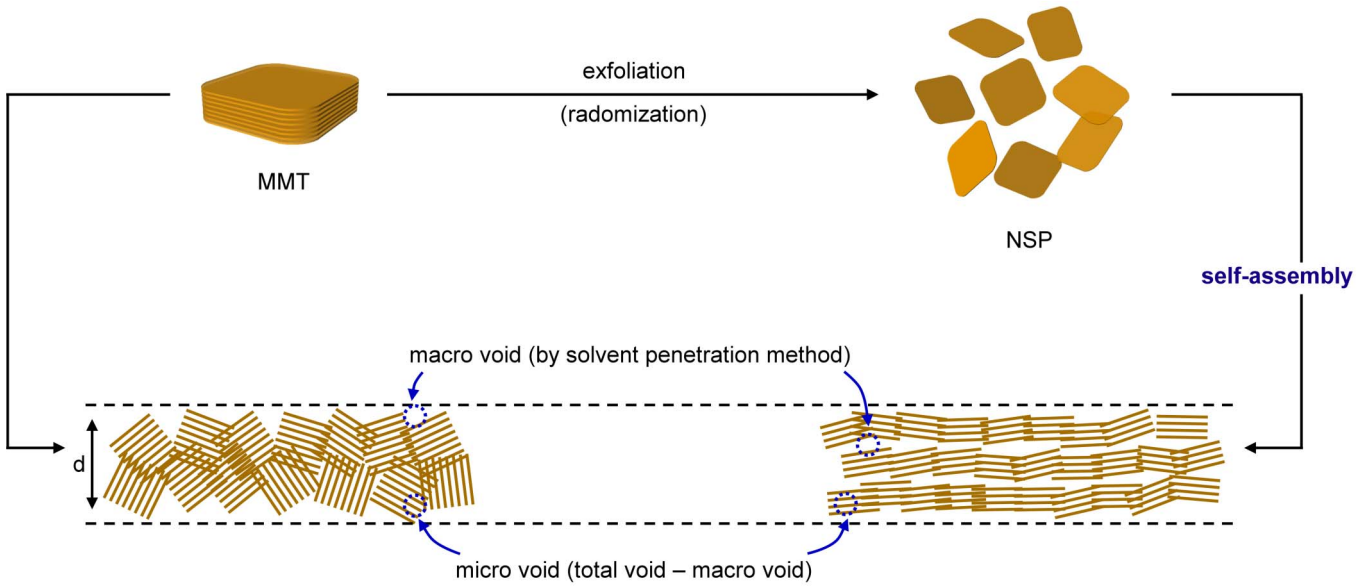

Figure 3 | Fundamental units and air voids in alternating multilayered structures of NSP and MMT films. Differences in the nanostructures of the MMT and NSP films from the units of MMT clay stacks and NSPs, and a conceptual illustration of macro and micro voids in both types of films (d = film thickness).

pristine MMT film failed to block a flame for longer than 30 seconds because the flame punctured the film. After the exposure to fire, the surface looked wrinkled and displayed large overlapping domains around the burned holes that were reminiscent of fish scales (Fig. 4a). By comparison, the NSP film maintained its original morphology on the flame-contacted area, showing minimal coarsening and damage in texture (Fig. 4b). Further observation by SEM showed tiny holes and uneven thermal expansion of the microstructures on the surface of the MMT film (Fig. 4c). On the other hand, the microstructures of the NSP film were only slightly affected by the flame treatment (Fig. 4d). More importantly, the flame propagation along a NSP film was confined to a circle of 5 cm in radius after one hour of exposure to the flame (see Supplementary Fig. S3 and Movies 2 online). By comparison, NSPs with water-soluble poly(vinyl alcohol) as a binder retained flame-blocking capability to a less extent and produced burning smoke.

We evaluated the flame-shielding capability by placing a cotton ball one centimeter behind a film and applying a butane gas-torch flame with a temperature greater than 1000°C from the other side of the film. As the control, the MMT film failed to protect the cotton ball because the film surface was punctured by the flame within ten seconds (Fig. 4e). By comparison, the NSP film protected the cotton ball from a continuous flame for over an hour (Fig. 4f). We did not expect this kind of protection for NSP films as thin as 20 μm. The MMT films could block a flame only for short times (2 to 30 seconds), even when their thicknesses were increased from 20 to 100 μm. A video shows a thin and flexible NSP film protecting a cotton ball from a flame (see Supplementary Movies 3 online).

The thermal histories of the films against a continuous flame were plotted against time (Fig. 5 and see Supplementary Fig. S4 online for setup). The large temperature differences measured between the two sides of the NSP films indicate efficient shielding of heat. The temperature over 700°C on the flame-contacted area and the temperatures of 210 to 230°C on the opposite sides of the films were measured by two thermocouples that touched the films after five minutes of stable burning. Interestingly, the thermocouple one centimeter away from the back of the NSP films measured a temperature of only 55°C, which remained constant during the hour-long experiments. Surprisingly, the NSP film that was 20 μm thick outperformed the thicker 100 μm film. The heat-shielding of the NSP films can be attributed to their low thermal conductivities (0.17 to 0.30 $W\ m^{-1}\ K^{-1}$ for thicknesses of 20 and 100 μm, respectively). The measurement was one tenth of the value reported in the literature, 2.93 $W\ m^{-1}\ K^{-1}$, for clay minerals[29,30].

We hypothesize that the heat-blocking ability of the NSP films largely depends on their volume fraction of air voids. The nanostructure of the 20 μm NSP film has a higher volume fraction (42%) than that of the 100 μm film (31%). The efficient heat shielding in the *z*-direction appears to arise primarily from the micro voids in the nanostructure. Overall, the platelet-to-platelet regularity of stacked NSPs, which creates alternating layers of voids in the nanostructure, contributes most to the ability of the films to block a flame and heat.

Table 2 | Estimation of volumes of macro and micro voids in the clay films by two density measurements

	Thickness (μm)	Bulk density ($g\ cm^{-3}$)	Apparent density ($g\ cm^{-3}$)	Total void (%)	Micro void (%)	Macro void (%)	Micro/Macro ratio
Silicate bulk	–	2.6	–	–	–	–	–
MMT film	20	1.5	2.2	42	10	32	0.31
	55	1.8	2.2	31	13	18	0.72
	87	2.0	2.2	23	14	9.0	1.6
	110	2.1	2.3	19	11	8.0	1.4
NSP film	19	1.5	2.1	42	14	28	0.50
	55	1.7	2.0	35	20	15	1.3
	86	1.8	1.9	31	26	5.0	5.2
	110	1.8	1.9	31	26	5.0	5.2

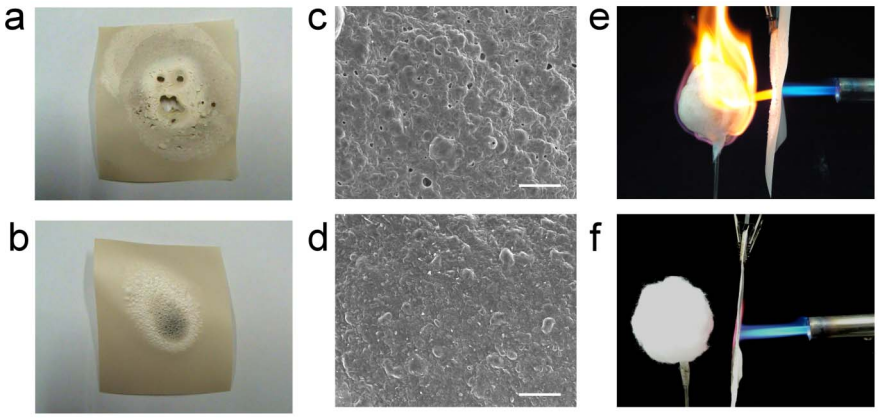

Figure 4 | Topologies of the clay films after exposure to a flame, and flame shielding. After exposure to a flame: (a) Wrinkled and porous surface of an MMT film, (b) Surface of an NSP film, (c) SEM image of the surface of an MMT film (scale bar: 20 μm), and (d) SEM image of the surface of an NSP film (scale bar: 20 μm). Flame-shielding: (e) A flame penetrating an MMT film within 30 seconds, and (f) An intact cotton ball shielded from a flame for 60 minutes by an NSP film.

The controlled alignment of NSPs and the ultimate nanostructure with multiple layers of air voids confer to the films an excellent degree of both flame- and heat-shielding behavior.

Discussion

Nearly 100% inorganic, randomly dispersed NSPs align regularly into a planar orientation to produce a flexible and highly-ordered, continuously layered structure, as shown by SEM (Fig. 1e). In contrast, pristine MMT clay with the same composition of silicate platelets, but with a different primary unit of stacks, could self-assemble only into a less ordered nanostructure. During the evaporation of water, the bulky stacks settle on the substrate in a less regular manner. As more stacks deposit on a preceding layer, the layered structure of MMT films becomes wavy and poorly aligned. In contrast, exfoliated NSPs that serve as the most fundamental units disperse well in water. With an extensively charged surface and a large aspect ratio, the NSPs tend to self-assemble into a highly regular alignment of platelets. These differences in the regularity of stacking from different primary units were substantiated by SEM and XRD.

The self-assembly of NSPs in water produced highly ordered nanostructures that were able to block a flame and heat. With a large volume percentage of air entrapped in their multilayered nanostructure, the NSP films can effectively shield a flame at 1000°C. In contrast, the MMT films are vulnerable to flame exposure, instantly suffering the generation of pin-holes. With respect to blocking heat, the efficiency is explained by a low thermal conductivity, which ranges from 0.17 to 0.30 W m^{-1} K^{-1}. The low conductivity is attributed to the macro and micro voids present at approximately a 40 volume percentage in the alternating composite nanostructure.

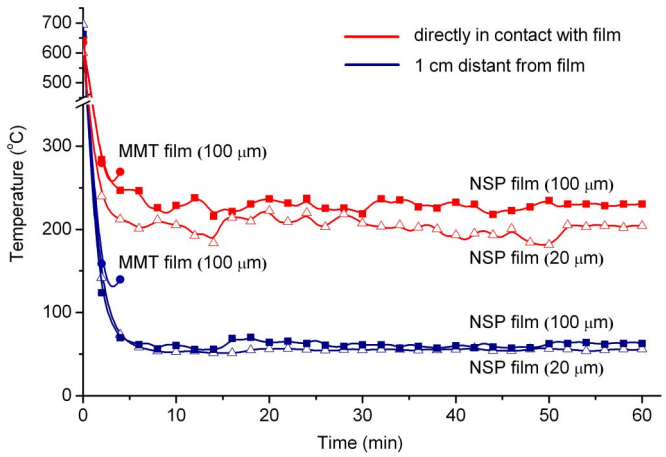

Figure 5 | Efficacy of heat shielding by the clay films. The ability to shield heat was measured by the difference in temperature of the side exposed to a flame and the backside of the film.

We found that the process of self-assembly could be scaled up to an area as large as 50 cm × 65 cm, while homogeneity was retained in the self-assembling of NSP units. Furthermore, we demonstrated that homogeneous and large-scale inorganic films can be fabricated by blending NSPs with poly(vinyl alcohol) (up to 50% in weight) to increase the flexibility of the films. The composite films have inferior flame-blocking capability and produced burning smoke.

The tendency of NSPs to self-assemble into multilayered nanostructures makes possible the easy fabrication of clay films that are large and flexible. The unique composition of 40 volume percentage of voids that alternate in a layered silicate structure should lead to new devices that block gas, heat, and flame.

Methods

Materials. Sodium montmorillonite (Na^+-MMT), a layered silicate clay with a cationic exchange capacity (CEC) of 1.20 mequiv g^{-1}, was supplied from Nanocor Co., USA. The 2/1 type of the natural smectite clays are aggregates from unit stacks of approximately 8–10 platelets in one stack. The individual silicate platelets were obtained from randomization of the clay through a previously developed exfoliation process, as described below.

Exfoliation of layered silicate Na^+-MMT into random platelets suspended in water. The preparation of NSPs from the exfoliation of Na^+-MMT by using polyamine quaternary salts has been reported previously. The exfoliated platelets could be extracted with two-phase toluene/NaOH to remove the organic exfoliating agents. The aqueous phase containing the suspended silicate platelets was separated and purified. The isolated NSP material, with ionic charges of ca. 18,000 ions per plate in the form of $\equiv SiO^-Na^+$, was hydrophilic and gelled in water, and it was estimated to be ca. 100 × 100 × 1 nm^3 in dimensions.

Preparation of an aqueous suspension of clay. To a four-necked round-bottomed flask (2000 mL) equipped with a mechanic stirrer, a reflux condenser, and a thermometer was added deionized water (1000 mL). Na^+-MMT (50 g) was added in one portion at ambient temperature. The mixture was brought to 80°C with vigorous stirring for 30 min to produce a homogenous aqueous suspension of Na^+-MMT. The NSP suspension was prepared according to our previous reports and diluted with deionized water to 5 wt% of clay content.

Preparation of the large free-standing film. The clay film was prepared by controlling the evaporation of water from aqueous dispersions of the clays. After being mechanically stirred for 30 min at 20 or 60°C, as specified by the experimental condition, the aqueous dispersion was cast onto a poly(ethylene terephthalate) tray. The dispersion was allowed to dry completely at either 25 or 60°C, according to the specified condition, to produce a homogeneous and uniform film.

Characterization. X-ray powder diffraction (XRD) was performed on a Schimadzu SD-D1 diffractometer with a Cu target ($\lambda = 1.5405$ Å) at a generator voltage of 35 kV, a generator current of 30 mA, and a scanning rate of 2°/min. The *d*-spacing ($n = 1$) was assigned on the basis of Bragg's equation: $n\lambda = 2d\sin\theta$. Two-dimensional wide-angle X-ray diffraction (2D-XRD) was performed on a Bruker D8 Discover with a two-dimensional Vantec-2000 area detector, which is a xenon-based gaseous avalanche detector with an active area of 14 cm × 14 cm (2048 pixel × 2048 pixel) with a spatial resolution of 68 um^2 on the area detector. The diffraction angle resolution is 0.02° with a collection time of 600 second. Scanning electron microscopy (SEM) was performed on a JEOL JSM-5600 SEM system and operated at 15 kV. The samples were coated with Pt before the SEM measurements. The thermal properties were analyzed by thermal gravimetric analysis (TGA) on a Perkin-Elmer Pyris 1 model. The organic content was estimated from the weight losses by ramping the temperature from 100 to 850°C at a rate of 10°C/min in air. The thermal conductivity of the samples was measured by using NanoFlash Apparatus on a NETZSCH Instruments LFA 447 model. The Xenon flash lamp fired a pulse at the sample's lower surface, while the infrared detector measured the temperature rise of the sample's top surface. Room-temperature (25°C) measurements of thermal diffusivity (±3%) and heat capacity (accuracy = ±5%) yielded thermal conductivity with an accuracy of ±9%

In the measurement of the bulk density (ρ_1), the mass (M_1) of the sample was determined on a Mettler Toledo analytical balance with a resolution of 0.0001 g. The thickness (T_1) of the sample was determined by averaging three measurements on different areas of the sample by using a micrometer (Fisher) with a resolution of 0.001 mm. The length (L_1) and width (W_1) of the sample were determined by averaging three measurements on different areas of the sample for each side using a digital caliper (Fisher) with a resolution of 0.001 mm. The bulk density was calculated according to equation (1): $\rho_1 = M_1/V_1$, where $V_1 = T_1 \times L_1 \times W_1$. The overall resolution for the bulk density measurement was 0.0001 g cm^{-3}.

In the measurement of the apparent density (ρ_2), the mass (M_2) of the sample was determined on a Mettler Toledo analytical balance with a resolution of 0.0001 g. The mass of the sample used in each measurement was in the range of 4.3000 to 4.7000 g. The volume (V_2) of the sample was measured in a 50.0 cm^3 burette (tolerance = 0.1 cm^3) prefilled with toluene by immersing the pre-weighed sample into the solvent and comparing the difference between the starting and final volume. The apparent density was calculated according to equation (2): $\rho_2 = M_2/V_2$.

With the above parameters ρ_1 and ρ_2, we estimated the total void volume percentage according to equation (3): $TV = (1/\rho_1 - 1/2.6)/V_1$, where 2.6 is the density of bulk MMT. The volume percentages of micro voids (Mi) and macro voids (Ma) could be calculated by equation (4): $Mi = (1/\rho_2 - 1/2.6)/V_1$ and equation (5): $Ma = (1/\rho_1 - 1/\rho_2)/V_1$, respectively.

1. Whitesides, G. M. & Grzybowski, B. Self-assembly at all scales. *Science* **295**, 2418–2421 (2002).
2. Bates, F. S. & Fredrickson, G. H. Block copolymer thermodynamics: theory and experiment. *Annu. Rev. Phys. Chem.* **41**, 525–557 (1990).
3. Hayward, R. C. & Pochan, D. J. Tailored assemblies of block copolymers in solution: it is all about the process. *Macromolecules* **43**, 3577–3584 (2010).
4. Kuo, S. W. Hydrogen bond-mediated self-assembly and supramolecular structures of diblock copolymer mixtures. *Polym. Int.* **58**, 455–464 (2009).
5. Haraguchi, K. & Takehisa, T. Nanocomposite hydrogels: a unique organic-inorganic network structure with extraordinary mechanical, optical, and swelling/de-swelling properties. *Adv. Mater.* **14**, 1120–1124 (2002).
6. Tetsuka, H., Ebina, T. & Mizukami, F. Highly luminescent flexible quantum dot–clay films. *Adv. Mater.* **20**, 3039–3043 (2008).
7. Rao, Y. & Blanton, T. N. Polymer nanocomposites with a low thermal expansion coefficient. *Macromolecules* **41**, 935–941 (2008).
8. Haraguchi, K. & Li, H. J. Control of the coil-to-globule transition and ultrahigh mechanical properties of PNIPA in nanocomposite hydrogels. *Angew. Chem. Int. Ed.* **44**, 6050–6054 (2005).
9. Podsiadlo, P. *et al.* Ultrastrong and stiff layered polymer nanocomposites. *Science* **318**, 80–83 (2007).
10. Ebina, T. & Mizukami, F. Flexible transparent clay films with heat-resistant and high gas-barrier properties. *Adv. Mater.* **19**, 2450–2453 (2007).
11. Tetsuka, H., Ebina, T., Tsunoda, T., Nanjo, H. & Mizukami, F. Flexible organic electroluminescent devices based on transparent clay films. *Nanotechnology* **18**, 355701–355704 (2007).
12. Priolo, M. A., Gamboa, D. & Grunlan, J. C. Transparent clay-polymer nano brick wall assemblies with tailorable oxygen barrier. *ACS Appl. Mater. Interfaces* **2**, 312–320 (2010).
13. Shikinaka, K. *et al.* Flexible, transparent nanocomposite film with a large clay component and ordered structure obtained by a simple solution-casting method. *Langmuir* **26**, 12493–12495 (2010).
14. Priolo, M. A., Gamboa, D., Holder, K. M. & Grunlan, J. C. Super gas barrier of transparent polymer-clay multilayer ultrathin films. *Nano Lett.* **10**, 4970–4974 (2010).
15. Nam, H. J., Ebina, T. & Mizukami, F. Formability and properties of self-standing clay film by montmorillonite with different interlayer cations. *Colloids and Surfaces A: Physicochem. Eng. Aspects* **346**, 158–163 (2009).
16. Walther, A. *et al.* Facile access to large-scale, self-assembled, nacre-inspired, high-performance materials with tunable nanoscale periodicities. *ACS Appl. Mater. Interfaces* **5**, 3738–3747 (2013).
17. Lu, S. Y. & Hamerton, I. Recent developments in the chemistry of halogen-free flame retardant polymers. *Prog. Polym. Sci.* **27**, 1661–1712 (2002).
18. Kiliaris, P. & Papaspyrides, C. D. Polymer/layered silicate (clay) nanocomposites: An overview of flame retardancy. *Prog. Polym. Sci.* **35**, 902–958 (2010).
19. Walther, A. *et al.* Supramolecular control of stiffness and strength in lightweight high performance nacre-mimetic paper with fire-shielding properties. *Angew. Chem. Int. Ed.* **49**, 6448–6435 (2010).
20. Walther, A. *et al.* Large-area, lightweight and thick biomimetic composites with superior material properties via fast, economic, and green pathways. *Nano Lett.* **10**, 2742–2748 (2010).
21. Yao, H. B., Tan, Z. H., Fang, H. Y. & Yu, S. H. Artificial nacre-like bionanocomposite films from the self-assembly of chitosan–montmorillonite hybrid building blocks. *Chem. Int. Ed.* **49**, 10127–10131 (2010).
22. Liu, A., Walther, A., Ikkala, O., Belova, L. & Berglund, L. A. Clay Nanopaper with tough cellulose nanofiber matrix for fire retardancy and gas barrier functions. *Biomacromolecules* **12**, 633–641 (2011).
23. Lin, J. J., Chu, C. C., Chiang, M. L. & Tsai, W. C. First isolation of individual silicate platelets from clay exfoliation and their unique self-assembly into fibrous arrays. *J. Phys. Chem. B* **110**, 18115–18120 (2006).
24. Lin, J. J., Chu, C. C., Chou, C. C. & Shieu, F. S. Self-assembled nanofibers from random silicate platelets. *Adv. Mater.* **17**, 301–304 (2005).
25. Chiu, C. W. & Lin, J. J. Self-assembly behavior of polymer-assisted clays. *Prog. Polym. Sci.* **37**, 406–444 (2012).
26. Liu, T., Chen, B. & Evans, J. R. G. Ordered assemblies of clay nano-platelets. *Bioinsp. Biomim.* **3**, 016005 (2008).
27. Walley, P., Zhang, Y. & Evans, J. R. G. Self-assembly of montmorillonite platelets during drying. *Bioinspir. Biomim.* **7**, 046004 (2012).
28. Osman, M. A., Mittal, V. & Lusti, H. R. The aspect ratio and gas permeation in polymer-layered silicate nanocomposites. *Macromol. Rapid Commun.* **25**, 1145–1149 (2004).
29. Rees, S. W., Zhou, Z. & Thomas, H. R. The influence of soil moisture content variations on heat losses from earth-contact structures: an initial assessment. *Build. Environ.* **36**, 157–165 (2001).
30. De Vries, D. A. *Physics of Plant Environment* (North-Holland Publishing Co., Amsterdam, 1966).

Acknowledgements

We acknowledge financial support from the Ministry of Economic Affairs and the National Science Council (NSC) of Taiwan.

Author contributions

J.J.L. conceived the general ideas, designed the experiments, and revised the manuscript. Y.C.W. and T.K.H. performed the experiments and wrote the manuscript. S.H.T. and T.M.W. interpreted the XRD data.

Additional information

Supplementary information accompanies this paper at http://www.nature.com/scientificreports

Competing financial interests: The authors declare no competing financial interests.

How to cite this article: Wang, Y., Huang, T., Tung, S., Wu, T. & Lin, J. Self-assembled clay films with a platelet–void multilayered nanostructure and flame-blocking properties. *Sci. Rep.* **3**, 2621; DOI:10.1038/srep02621 (2013).